

Highlight Model of Underwater Target Acoustic Scattering in the Bistatic System

Zhao-Ran Meng*, Yang Song, Fu-Xiang Yu, Chun-Lei Zhang, Yu-Qiang Zhang

Dalian Scientific Test and Control Technology Institute, Dalian 116013, China

mengzhaoran99@163.com

Received 27 March 2024; Revised 8 April 2024; Accepted 15 April 2024

Abstract. A highlight model for the target signal in the bistatic system is proposed based on the calculation results of the acoustic field, which means that the target can be equivalent to several highlights according to certain characteristics of the target when calculating the scattering acoustic field. The parameters of the highlight model were given based on the calculation results. Two sets of experiments on the highlight model of the bistatic system were conducted with a fixed transmitter and a target, one being the receiver rotating around the target, and the other being the target rotating around itself at different receiver angles. The comparison of multi angle pseudo color images through experiments and theoretical simulations shows that the scattering highlight model can describe the scattering characteristics of the target to a certain extent. Only geometric highlights were simulated in this article, and it can be foreseen that bistatic system highlight model of scattering waves can be accurately described with a full understanding of the target.

Keywords: highlight model, acoustic, bistatic system, theoretical simulations, cylindrical targets

1 Introduction

At present, the theoretical research on the scattering sound field of the target is attributed to the mathematical physics problem, which refers to the solution of the acoustic scattering field of the target in the three-dimensional space excited by the acoustic wave after satisfying the corresponding boundary conditions, radiation conditions and wave equations.

It is precisely because the research on the scattering sound field of the target is solved and analyzed by the wave equation under the specific boundary, the solution to the accurate solution of the acoustic scattering theory is obtained, that is, the mathematical principle of the Huygens principle is explained by the Helmholtz-Kirchhoff integral formula, and the acoustic scattering field of the whole target is obtained by using the integral equation. In the whole process, the scatterer studied is regarded as an active sound source. The exact solution obtained by this method is to simplify the volume integral into the area integral, so as to solve the sound field through the sound pressure and normal vibration velocity on the integrated surface.

Based on physical acoustic method, the signal highlight model for the target of the monostatic system has long been proposed and widely applied under the condition of short pulse [1]. The acoustic field of the bistatic system varies with the split angle, which makes the relevant calculations more complex. In recent years, there has been an increasing trend in research on bistatic system [2-11], which has the following characteristics: the analysis of spherical targets is more than other types, and the theoretical examples are more than the experimental verification. This article conducts experimental measurements based on the calculation results of the scattered acoustic field of cylindrical targets, and the theoretical results were compared and analyzed with the experimental results.

In reference [12], a highlight model was proposed based on the analysis results of the monostatic system, which equates a complex target to several highlights, each of which has three main factors: amplitude, delay, and phase. The highlight model is generally used to describe the target echo in a monostatic system [13-18].

For a bistatic system, it can be considered that the scattered sound of the target is related to the characteristics of the incident sound and the target (including the surrounding environment) itself. For cases where the incident sound is of small amplitude, it is considered that the incident sound and scattered sound are inputs and outputs of a linear system (related to the target and environment), and are independent of the initial time of the incident. Similar to a monostatic system, this article believes that the signals received by a bistatic system can also be described using highlight model.

* Corresponding Author

2 Elements of Highlight Model

For a monostatic system the echo can be described by the equivalent highlights of the target which calculated only in a certain direction because the transmitter and receiver are in the same position.

The main difference between split systems is that as the split angle changes, the characteristics of the highlights will have significant differences, so the issues that need to be considered need to be more complex. While in bistatic systems the issues that need to be considered need to be more complex because that the characteristics of the highlight model such as the appearance time, amplitude, and delay will have significant differences as the split angle changes. In theory, at any split angle condition in a bistatic system, the scattered wave of the target can be represented by the superposition of several highlights as follows:

$$H(\vec{r}, \omega) = \sum_{m=1}^N A_m(\vec{r}, \omega) e^{i\omega\tau_m} e^{i\phi}. \quad (1)$$

The three main parameters are amplitude, delay, and phase in the highlight model of the monostatic system. The highlight model of the bistatic system is defined in a similar way, and the key is to calculate the theoretical highlights information of the target. Generally speaking, highlights should include all information about the target. According to existing theories, scattering highlights are mainly composed of geometric highlights and elastic highlights.

The analysis of elastic highlights requires calculating the elastic scattering of the target. Taking quasi-Lamb wave as an example, elastic cylindrical targets are only excited under certain specific conditions. For the convenience of verification, this paper only calculates the geometric highlights of the main components of the cylinder target, and does not include the elastic highlights. Geometric highlights as the main highlights are the focus of this paper.

2.1 Calculation of Highlight Model About Rigid Finite Cylindrical Target in Monostatic

The basic principle of Kirchhoff approximation is to approximate the calculation of high-frequency acoustic scattering as optical calculation. The application of this approximation needs to meet two conditions: first, the contribution of the shadow area is not considered in the calculation, and the integral surface used in the actual calculation is the surface that can be observed at both the transmitting point and the receiving point. Secondly, the following formulas can be applied to the surface of the rigid target:

$$\begin{cases} \Phi_s = \Phi_i \\ \Phi_s / \partial n = -\Phi_i / \partial n \end{cases} \quad (2)$$

The formula of the highlight model about cylindrical target is derived according to the Kirchhoff approximation. For monostatic situation, with the time factor $e^{-i\omega t}$ omitted, the scatter field is expressed as follows:

$$\phi_s = \frac{iAk}{2\pi} \iint_S \frac{1}{r^2} e^{2ikr} \cos(r, n) dS. \quad (3)$$

Where the propagation effect is removed and the target size is assumed to be much smaller than the distance between the target and the sound source. Under this condition:

$$r^2 = r_0^2. \quad (4)$$

According formula (3) we let integral term in the equation

$$I = \int_S e^{2ik\Delta r} \cos \Theta ds. \tag{5}$$

Where S is the surface which could be seen in monostatic point. Δr is the difference between the sound path and the reference point. $\cos \Theta$ is the angle between the incident (reflection) direction and the target surface normal. ds is area element. It is assumed that the plane wave is incident when calculating the integral.

In order to understand the calculation, we start with a simple target, a rigid sphere. For rigid sphere target in monostatic situation, the integral surface is shown in Fig. 1, if $ka \gg 1$:

$$\begin{aligned} I &= \int_0^\pi e^{-2ika \cos \theta} \cos \theta 2\pi a^2 \sin \theta d\theta = 2\pi a^2 \int e^{-2ika \cos \theta} \cos \theta \sin \theta d\theta \\ &= 2\pi a^2 \times \frac{1}{4} \frac{e^{-2ika} (2ika + 1 - e^{2ika})}{a^2 k^2} \approx e^{-2ika} \frac{\pi a^2}{2} \frac{2i}{ka} = \frac{i\pi a}{k} e^{-2ika}. \end{aligned} \tag{6}$$

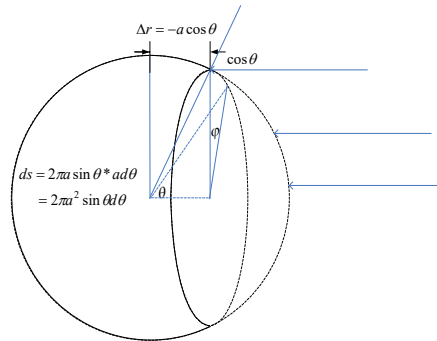


Fig. 1. The range of integration in monostatic

The placement of columns and calculation parameters are shown in the Fig. 2. Where the acoustic path difference between the center of the front face and the center of the cylinder is $L \cos \alpha / 2$, and the acoustic path difference between the center of the front face and anywhere of the front face is $r \cos \theta \sin \alpha$, r is the polar radius of the end face in the polar coordinates. θ is the polar angle in the polar coordinates. So,

$$\Delta r = -(r \cos \theta \sin \alpha + \frac{L}{2} \cos \alpha). \tag{7}$$

For the calculation of the front face let $\gamma = kL \cos \alpha$ and $\beta = 2ka \sin \alpha$ for two reasons. One reason is to be convenience for calculating. The other reason is if γ and β are divided by k the answers are the acoustic path difference of front face to target center and summit to front face center. For the front face,

$$I_D = \int_0^a \int_0^{2\pi} e^{-2ik(r \cos \theta \sin \alpha + \frac{L}{2} \cos \alpha)} \cos \alpha r dr d\theta = 2\pi a^2 e^{-i\gamma} \frac{\gamma}{kL\beta} J_1(\beta). \tag{8}$$

If $\alpha = 0$, $I = \pi a^2 e^{-ikL}$.

For the side surface,

$$I_L = \int_0^\pi \int_0^L e^{-2ik(\frac{L}{2} \cos \alpha - l \cos \alpha + a \sin \theta \sin \alpha)} a \sin \theta \sin \alpha dl d\theta = \frac{1}{2k} \frac{L \sin \gamma}{\gamma} \beta \pi (\frac{2}{\pi} - iJ_1(\beta) - S_1(\beta)). \tag{9}$$

Where S_1 is the Struve function. The highlight model about rigid finite cylindrical target in monostatic is

$$I = I_D + I_L. \quad (10)$$

If $\beta \gg 1$ we have:

$$J_1(\beta) = \sqrt{\frac{2}{\pi\beta}} \cos\left(\beta - \frac{3\pi}{4}\right). \quad (11)$$

$$S_1(\beta) = \sqrt{\frac{2}{\pi\beta}} \sin\left(\beta - \frac{3\pi}{4}\right) + \frac{2}{\pi}. \quad (12)$$

Then,

$$I_D = \frac{\pi a^2}{kL} \cdot \frac{\gamma}{\beta} \cdot \sqrt{\frac{2}{\pi\beta}} \left\{ \exp\left[-i\left(\beta + \gamma - \frac{3\pi}{4}\right)\right] + \exp\left[-i\left(\gamma - \beta + \frac{3\pi}{4}\right)\right] \right\}. \quad (13)$$

$$I_L = \frac{\pi L}{4k} \cdot \frac{\beta}{\gamma} \cdot \sqrt{\frac{2}{\pi\beta}} \left\{ \exp\left[-i\left(\beta + \gamma - \frac{3\pi}{4}\right)\right] + \exp\left[-i\left(\beta - \gamma - \frac{3\pi}{4}\right)\right] \right\}. \quad (14)$$

Compare formula (1) with (13) and (14) we can get the highlight model about rigid finite cylindrical target in monostatic. The amplitude is decided by $\frac{\pi a^2}{kL} \cdot \frac{\gamma}{\beta} \cdot \sqrt{\frac{2}{\pi\beta}}$ and $\frac{\pi L}{4k} \cdot \frac{\beta}{\gamma} \cdot \sqrt{\frac{2}{\pi\beta}}$, and delay is decided by $\beta + \gamma$ and $\pm(\beta - \gamma)$, phase is decided by $\frac{3\pi}{4}$. We got

$$\phi_s = \sum_{n=1}^3 \phi_{sn} = \frac{\phi_i}{4\pi} \cdot \frac{a}{r_0} \cdot e^{i2kr_0} \cdot \sum_{n=1}^3 R_n. \quad (15)$$

Where

$$R_1 = \sqrt{\frac{\pi}{ka}} \cdot \frac{1}{\sin^{3/2}\theta \cos\theta} \exp[-i(\beta + \gamma)] \exp\left(i\frac{\pi}{4}\right). \quad (16)$$

$$R_2 = \sqrt{\frac{\pi}{ka}} \cdot \frac{1}{\sin^{3/2}\theta} \exp[-i(\gamma - \beta)] \exp\left(i\frac{3\pi}{4}\right). \quad (17)$$

$$R_3 = \sqrt{\frac{\pi}{ka}} \cdot \frac{\sin^{1/2}\theta}{\cos\theta} \exp[-i(\beta - \gamma)] \exp\left(i\frac{5\pi}{4}\right). \quad (18)$$

The above results reflect the echo characteristics under the condition of narrow pulse. In contrast, if the pulse length is long enough, the steady-state response can be obtained, which is usually characterized by the target strength, that is

$$TS = \begin{cases} 10 \lg \left[\frac{aL^2}{2\lambda} \left(\frac{\sin \eta}{\eta} \right)^2 \cos^2 \alpha \right], \alpha \neq \frac{\pi}{2} \\ 10 \lg \left(\frac{aL^2}{2\lambda} \right), \alpha = \frac{\pi}{2} \end{cases} \quad (19)$$

Where $\eta = kL \sin \alpha$, λ is the wavelength of sound.

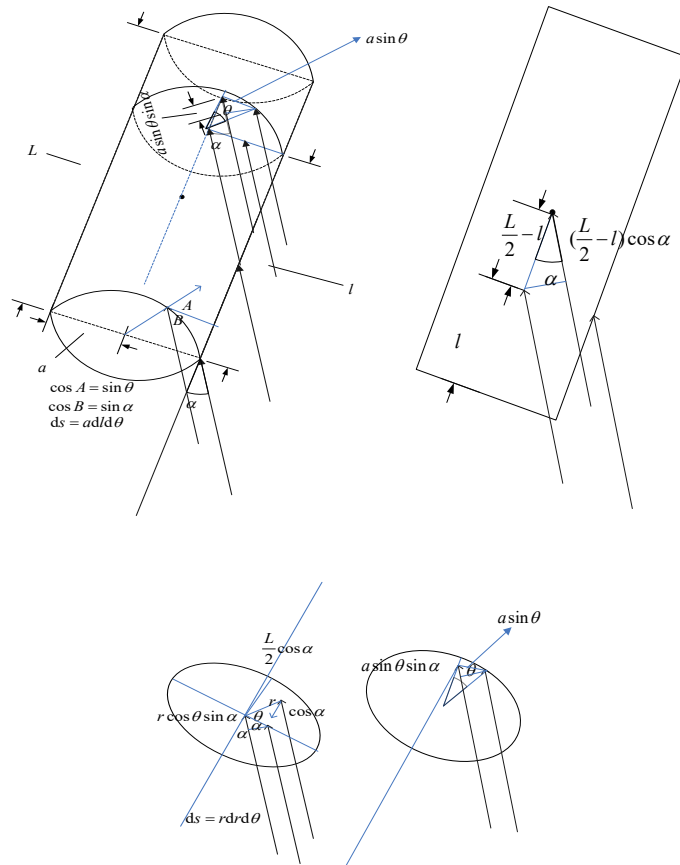


Fig. 2. Highlight model about cylindrical target in monostatic

2.2 Calculation of Highlight Model about Rigid Finite Cylindrical Target in Bistatic

The bistatic scattered sound field can be calculated by the following formula:

$$\phi_s = \frac{iAk}{4\pi} \iint_S \frac{1}{r_1 r_2} e^{ik(r_1+r_2)} [\cos(r_1, n) + \cos(r_2, n)] dS. \quad (20)$$

According to formula (20) we got:

$$\Phi = \frac{ike^{ikr_0}}{4\pi r_0^2} \iint_S e^{ik(\Delta r_1 + \Delta r_2)} (\cos \Theta_1 + \cos \Theta_2) dS. \quad (21)$$

The integral surface should be the dark area shown in Fig. 3. the polar angle φ is between 0 and π , the azimuth angle θ is the angle between transmit direction and reference surface. Omit the amplitude change caused by spherical wave propagation

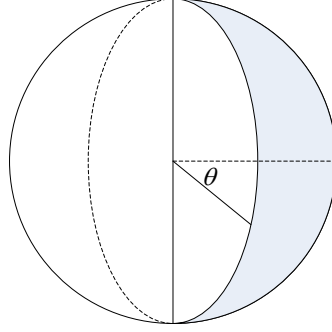


Fig. 3. The range of integration in bistatic

$$\begin{aligned} I &= \int e^{ik(\Delta r_1 + \Delta r_2)} (\cos \Theta_1 + \cos \Theta_2) ds \\ &= \int_{\alpha - \frac{\pi}{2}}^{\frac{\pi}{2}} \int_0^{\pi} e^{-ik(a \sin \varphi \cos \theta + a \sin \varphi \cos(\alpha - \theta))} (\sin \varphi \cos \theta + \sin \varphi \cos(\alpha - \theta)) a^2 \sin \varphi d\varphi d\theta \\ &= \iint e^{-2ika \sin \varphi \cos \frac{\alpha}{2} \cos(\theta - \frac{\alpha}{2})} 2 \cos \frac{\alpha}{2} \cos(\theta - \frac{\alpha}{2}) a^2 \sin^2 \varphi d\varphi d\theta. \end{aligned} \quad (22)$$

According to stationary phase point

$$I = \frac{i2\pi a}{k} e^{-2ika \cos \frac{\alpha}{2}}. \quad (23)$$

Through the preorder calculation and analysis, we can get the conclusion that the highlight model of the sphere is usually simpler, because it consists of only one item.

In contrast, the highlight model of the cylinder is more complicated. According to the different positions of the integral, in order to facilitate the calculation, the formula (21) can be divided into two parts, that is,

$$\Phi = \frac{ike^{ikr_0}}{4\pi r_0^2} (I_D + I_L). \quad (24)$$

Where $I_D = \iint_{S_D} e^{ik(\Delta r_1 + \Delta r_2)} (\cos \Theta_1 + \cos \Theta_2) dS$, $I_L = \iint_{S_L} e^{ik(\Delta r_1 + \Delta r_2)} (\cos \Theta_1 + \cos \Theta_2) dS$. Where I_D is the integral result of the end face of the cylinder, I_L is the integral result of the side face of the cylinder. The detailed integral surface is shown in Fig. 4.

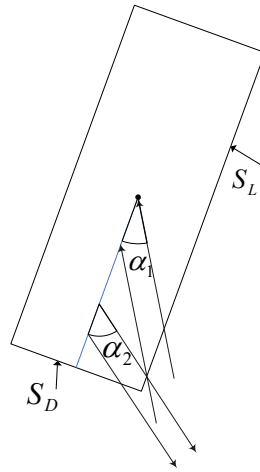


Fig. 4. Parameter definition for calculation of highlight model of cylindrical target

α_1 is the angle between the incident direction to the cylinder bus, and α_2 is the angle between the reflection direction to the cylinder bus, which are shown in Fig. 4. The geometric center of the column is taken as the starting point of the acoustic path calculation, the vector from the surface of the cylinder to the transmitter point is defined as \vec{s} , the vector from the surface of the cylinder to the receiver point is defined as \vec{r} . The vector perpendicular to the axis of the cylinder and in the same plane with the transmitter and receiver is defined as \vec{l} . The vector perpendicular to the lower end face of the cylinder is defined as \vec{a} . Fig. 5 provides the definition of the above variables.

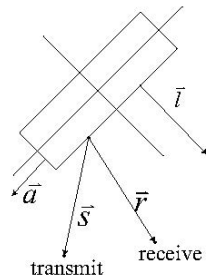


Fig. 5. The position relationship of each vector in the calculation

According to formula (24) we got

$$\begin{aligned}
 I_D &= \int_0^a \int_0^{2\pi} e^{-ik(r \cos \theta \sin \alpha_1 + \frac{L}{2} \cos \alpha_1)} e^{-ik(r \cos \theta \sin \alpha_2 + \frac{L}{2} \cos \alpha_2)} (\cos \alpha_1 + \cos \alpha_2) r dr d\theta \\
 &= e^{-ik \frac{L}{2} (\cos \alpha_1 + \cos \alpha_2)} (\cos \alpha_1 + \cos \alpha_2) \int_0^a \int_0^{2\pi} e^{-ikr \cos \theta (\sin \alpha_1 + \sin \alpha_2)} r dr d\theta.
 \end{aligned}
 \tag{25}$$

Let $\cos \alpha_1 + \cos \alpha_2 = 2 \cos A$, $\sin \alpha_1 + \sin \alpha_2 = 2 \sin B$, $\gamma = kL \cos A$, $\beta = 2ka \sin B$, we got

$$I_D = e^{-i\gamma} 2 \cos A \int_0^a \int_0^{2\pi} e^{-i2kr \sin B \cos \theta} r dr d\theta = 4\pi a^2 e^{-i\gamma} \frac{\gamma}{kL\beta} J_1(\beta).
 \tag{26}$$

Approximately

$$J_1(\beta) = \sqrt{\frac{2}{\pi\beta}} \cos\left(\beta - \frac{3\pi}{4}\right). \quad (27)$$

Take formula (11) into formula (26) got

$$\begin{aligned} I_D &= 4\pi a^2 e^{-i\gamma} \frac{\gamma}{kL\beta} J_1(\beta) \\ &= \frac{\cos A}{k \sin B} \sqrt{\frac{\pi a}{k \sin B}} \left\{ \exp[-i(\gamma + \beta) + \frac{3\pi}{4}i] + \exp[-i(\gamma - \beta) - \frac{3\pi}{4}i] \right\}. \end{aligned} \quad (28)$$

Where $\gamma + \beta$ and $\gamma - \beta$ correspond to the closest acoustic path point and the farthest acoustic path point on the circular end surface respectively.

If $\beta = 0$, according to $\beta = ka(\sin \alpha_1 + \sin \alpha_2)$, we got $\sin \alpha_1 + \sin \alpha_2 = 0$. It shows that the α_1 and α_2 are opposite numbers to each other, which indicates that mirror reflection occurs at the end face.

$$I_D = e^{-i\gamma} 2 \cos A \pi a^2. \quad (29)$$

The calculated result on the side of the cylinder is

$$\begin{aligned} I_L &= \iint_{S_L} e^{ik(\Delta r_1 + \Delta r_2)} (\cos \theta_1 + \cos \theta_2) dS = 2ae^{-i\gamma} \sin B \int_0^{\pi} \int_0^L e^{i2k \cos A l} e^{-i2k a \sin B \sin \theta} \sin \theta d\theta dl \\ &= \frac{L \sin \gamma}{k\gamma} \beta \pi \left(\frac{2}{\pi} - iJ_1(\beta) - S_1(\beta) \right). \end{aligned} \quad (30)$$

Take formula (11) and (12) into formula (30) got

$$I_L = \frac{\sin B}{k \cos A} \sqrt{\frac{\pi a}{k \sin B}} \left\{ \exp[-i(\beta + \gamma) + \frac{3\pi}{4}i] - \exp[-i(\beta - \gamma) + \frac{3\pi}{4}i] \right\}. \quad (31)$$

If $\gamma = 0$, according to $\gamma = kL(\cos \alpha_1 + \cos \alpha_2)/2$, we got $\cos \alpha_1 + \cos \alpha_2 = 0$. It shows that the two angles are complementary, which can be considered as mirror reflection at this time. For the calculation formula (31), there is

$$\lim_{\gamma \rightarrow 0} \frac{\sin \gamma}{\gamma} = 1. \quad (32)$$

Take formula (32) into formula (30) we got

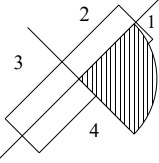
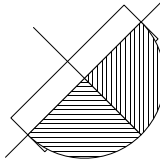
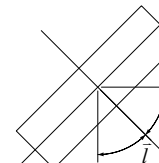
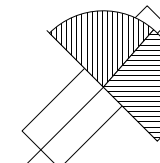
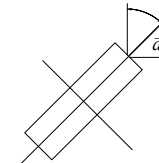
$$I_L = \frac{L}{k} \beta \pi \left(\frac{2}{\pi} - iJ_1(\beta) - S_1(\beta) \right) = \frac{L\sqrt{2\pi\beta}}{k} \exp[-i(\beta - \frac{\pi}{4})]. \quad (33)$$

Where $\gamma + \beta$ and $\gamma - \beta$ correspond to the closest acoustic path point and the farthest acoustic path point on the side of the cylinder respectively. Combine the results, we got

$$\begin{aligned} I_D + I_L &= \frac{1}{k \sin B \cos A} \sqrt{\frac{\pi a}{k \sin B}} \left\{ (\cos^2 A + \sin^2 B) \exp[-i(\beta + \gamma) + \frac{3\pi}{4}i] \right. \\ &\quad \left. + \cos^2 A \exp[-i(\gamma - \beta) - \frac{3\pi}{4}i] - \sin^2 B \exp[-i(\beta - \gamma) + \frac{3\pi}{4}i] \right\}. \end{aligned} \quad (34)$$

For cylindrical targets, the results can be separated into three items (i.e. three highlights), each with its own amplitude, time delay, and phase. Then a conclusion could be obtained which is shown in Table 1.

Table 1. The relationship between the highlight model of the cylinder and the system placement in the biastatic system

Sketch					
State	Transmitter and receiver are in the same quadrant	Transmitter and receiver are in two quadrants on the same side of the central axis	The angle between the transmitter and the \bar{l} is the same as the receiver	Transmitter and receiver are located on the same side of the center line perpendicular to the center axis	The angle between the transmitter and the \bar{a} is the same as the receiver
Result	$I_D + I_L$	I_L	I_L	I_D	I_D
Describe	Three highlights	Two highlights	One highlight	Two highlights	One highlight

Take Φ_0 into account we could get a result that includes the phase. As shown in Table 1, the three added terms determine the amplitude and phase of each highlight. The amplitude and phase of the scattering highlights of the target at any split angle are obtained from the perspective of the highlight model. The highlight model also has an important parameter which is the time when the received signal appears. In fact, this term has already been given in the equation, and the highlight model for cylindrical target is detailed below. The scattering field of cylindrical targets in the bistatic system needs to be discussed in three different cases according to the integral calculation in reference [19].

1. Only end face scattering. At this point, there should be two parts of signal, the acoustic paths are $r - (\gamma + \beta)/k$ and $r - (\gamma - \beta)/k$, the signal with smaller acoustic path arrives earlier, while signal with larger acoustic path arrives later.

2. Only lateral scattering. At this point, there should be two parts of signal, the acoustic paths are $r - (\gamma + \beta)/k$ and $r - (\beta - \gamma)/k$, the signal with smaller acoustic path arrives earlier, while signal with larger acoustic path arrives later.

3. Both end face and lateral scattering are included. In theory, there should be three parts of the signal, the acoustic paths are $r - (\gamma + \beta)/k$, $r - (\gamma - \beta)/k$ and $r - (\beta - \gamma)/k$. Among them, $r - (\gamma + \beta)/k$ is the smallest, and the other two acoustic paths are related to the placement position. Where r is the distance from the emission point to the target and then to the receiving point.

The signal occurrence time can be calculated based on the acoustic path. At this point, the three elements of the highlight model are obtained that is amplitude, time, and phase. From the above, it can be seen that theoretically, the scattering wave of bistatic system can also be calculated using the highlight model, and this article also provides results with clear physical significance for general objectives. In order to improve the highlight model theory of the bistatic system this article will use cylindrical targets as an example to experimentally verify the amplitude and time of this theory due to the importance of amplitude and time in practice.

3 The First Experiment of Sound Field Measurement in a Bistatic System

The experiment was conducted in a two-meter-deep channel water pool with anechoic tiles around and at the bottom of the pool. The acoustic centers of the cylindrical target, transmitting transducer, and receiving transducer are located on the same horizontal plane at a depth of 0.8m underwater, and the top view of their arrangement is shown in Fig. 6(a). The cylindrical target is a steel column shell with a wall thickness of 3.5mm, and its geometric parameters are shown in Fig. 6(b). The transmitted signal is a CW pulse with a pulse width of 0.15ms and a frequency of 100kHz. The opening angle of -3dB for transmitting and receiving transducer beams is 50 degrees. In the experiment, the direction of the transmitting transducer remains unchanged, and the cylinder forms an angle θ with the reference line ($\theta = 0, 30, 45, 60, 90$ degree). The receiving transducer rotates for half a circle with

a radius of 0.6m and the center of the target as the center. During the rotation process, the receiving beam always points towards the target, and ϕ is the angle between the receiver and the reference forward direction. The rotation process is manually adjusted, with each rotation of 1 degree. As can be seen from later analysis, it is precisely due to the manual method that certain errors are caused in the experiment. The experimental result is the signal amplitude which represented by a pseudo color image compared with the simulated signal.

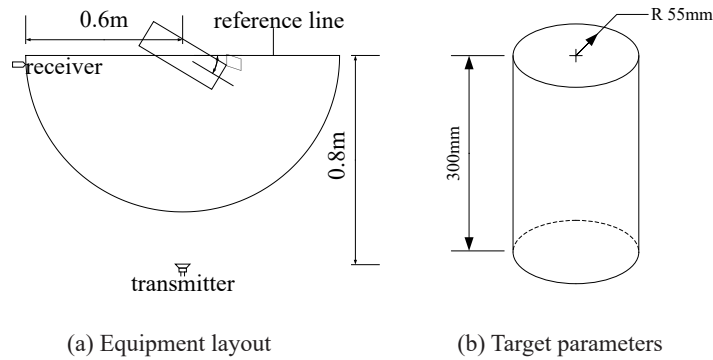
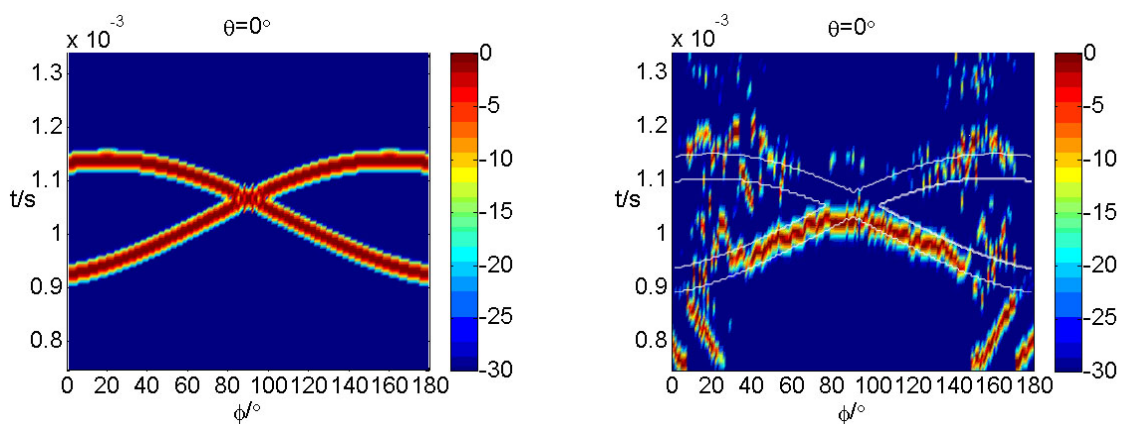


Fig. 6. Deployment of experiment and parameter of target

3.1 Comparison in Theoretical and Experimental with $\theta = 0^\circ$

In Fig. 7, the horizontal axis represents the angle between the receiver and the reference line, and the vertical axis represents the time from the transmission signal as the starting point. The pseudo color image shows the relative strength values of the received signal, Fig. 7(a) shows the simulation calculation results, and Fig. 7(b) shows the experimental measurement results.

There is only one highlight at $\phi = 90^\circ$ in theory. In the experiment, those slightly away from 90 degrees are still difficult to separate due to the difficulty in separating the two in terms of timing. The bright lines in the bottom left and bottom right of Fig. 7(b) represent direct sound signals which were not included in the simulation calculation. Scattering signals are almost invisible on both sides, due to the relatively small amount of scattered wave energy that can be received at this angle. Overall, the timing and relative amplitude of the highlights are in good agreement. The comparison of signals are shown in Fig. 8.



(a) Simulation calculation results of geometric highlights (b) Comparison of experimental and theoretical highlights

Fig. 7. Comparison in theoretical and experimental with $\theta = 0^\circ$

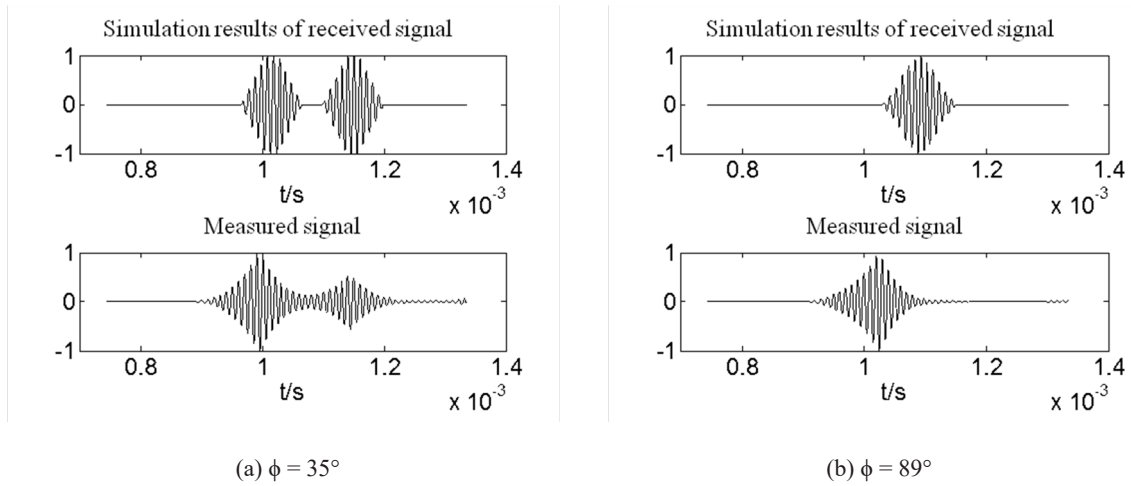
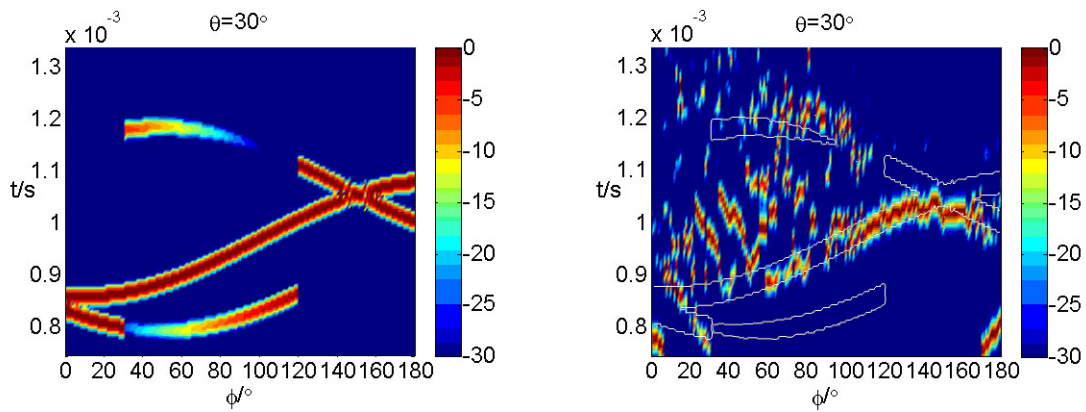


Fig. 8. Received signal of receiver with different angle

3.2 Comparison in Theoretical and Experimental with $\theta = 30^\circ$



(a) Simulation calculation results of geometric highlights (b) Comparison of experimental and theoretical highlights

Fig. 9. Comparison in theoretical and experimental with $\theta = 30^\circ$

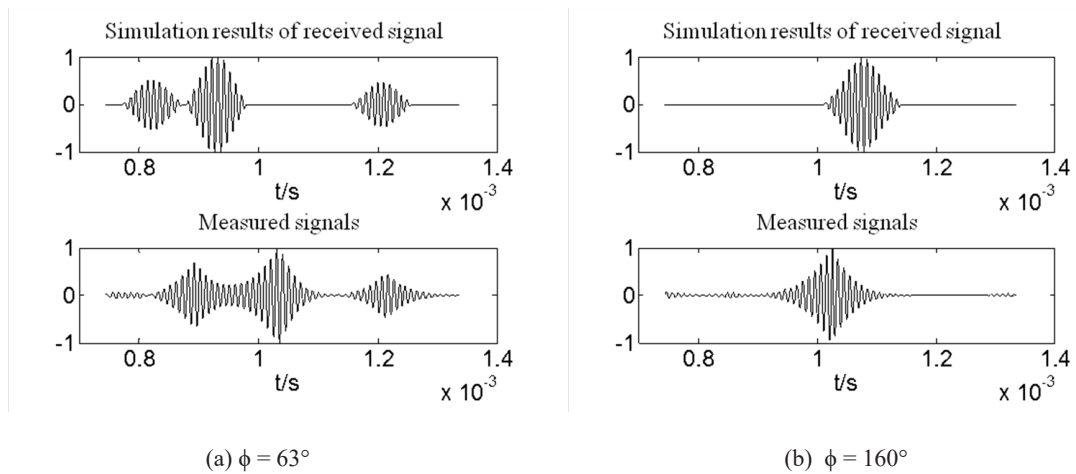
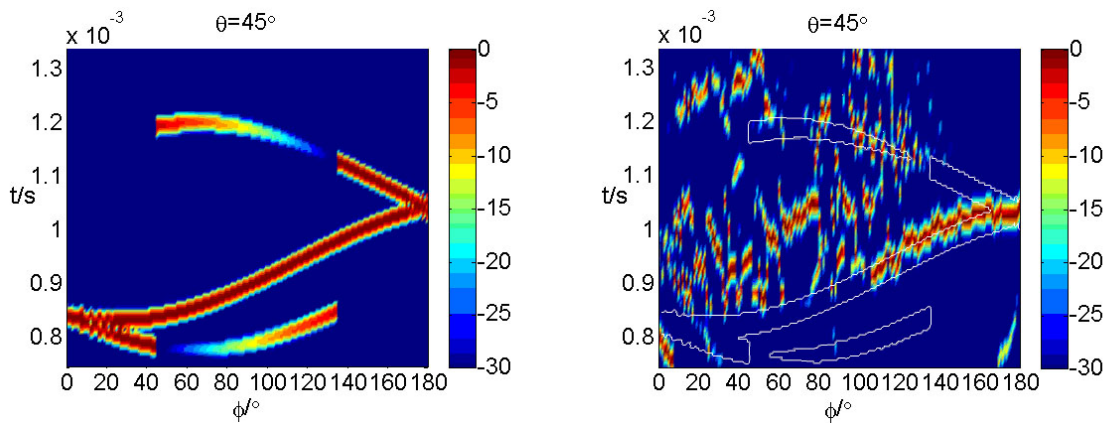


Fig. 10. Received signal of receiver with different angle

There is only one highlight in the mirror reflection area (150-degree), which is consistent with theoretical calculations in Fig. 9. While in Fig. 9(b), due to the large number of highlights, the graph becomes more complex. It can be seen that the time and amplitude can be well matched by comparing the theoretical waveform with the measured waveform at several angles. The comparison of signals are shown in Fig. 10.

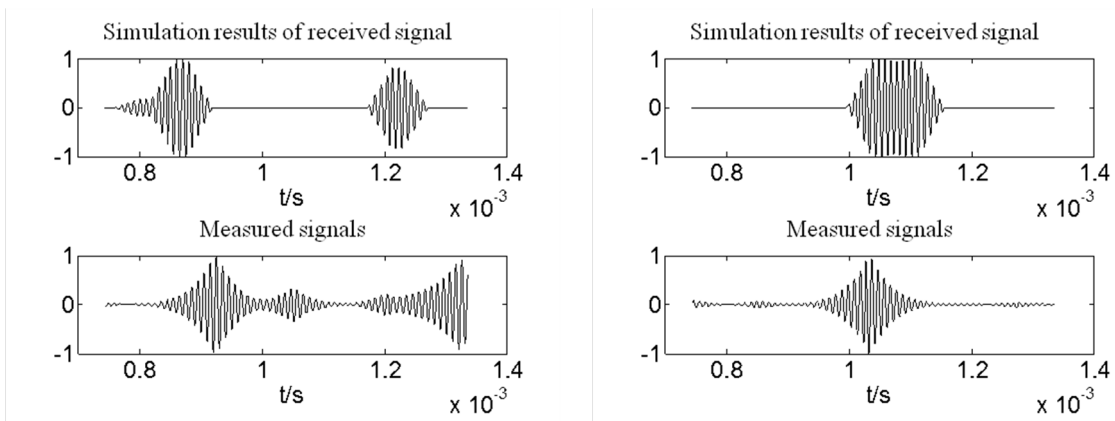
3.3 Comparison in Theoretical and Experimental with $\theta = 45^\circ$

When $\theta = 45^\circ$, the mirror reflection position is at $\phi = 180^\circ$, which is consistent with theory and experiment shown in Fig. 11 and Fig. 12. In theory, each signal is clearly separated, while in reality, it may appear chaotic in the image due to aliasing between signals. The theoretical and experimental results are in good agreement in the reflection area near the mirror, while other angles may be chaotic. This is due to the discontinuous rotation in the experiment and the high noise in the experimental environment.



(a) Simulation calculation results of geometric highlights (b) Comparison of experimental and theoretical highlights

Fig. 11. Comparison in theoretical and experimental with $\theta = 45^\circ$



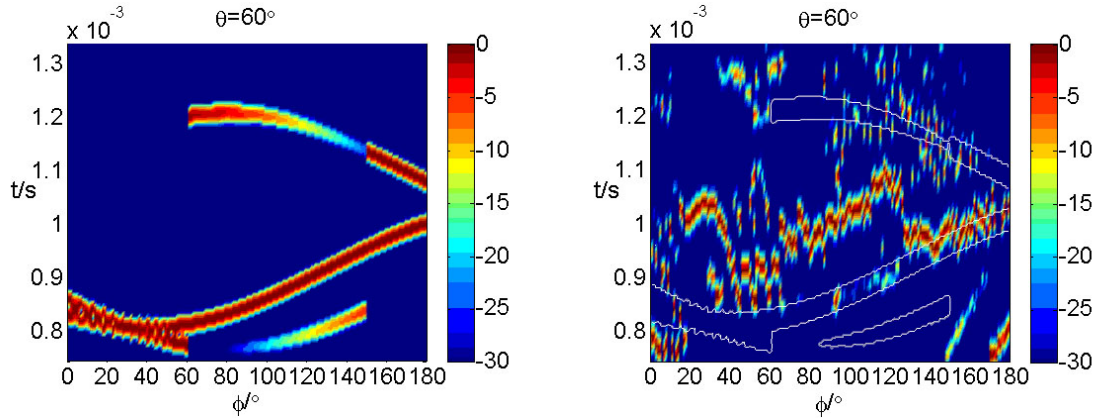
(a) $\phi = 50^\circ$

(b) $\phi = 160^\circ$

Fig. 12. Received signal of receiver with different angle

3.4 Comparison in Theoretical and Experimental with $\theta = 60^\circ$

At this point, the mirror reflection point is no longer visible. The position of the highlight at different reception angles is consistent with the theory. The comparison of highlights and signals are shown in Fig. 13 and Fig. 14.



(a) Simulation calculation results of geometric highlights (b) Comparison of experimental and theoretical highlights

Fig. 13. Comparison in theoretical and experimental with $\theta = 60^\circ$

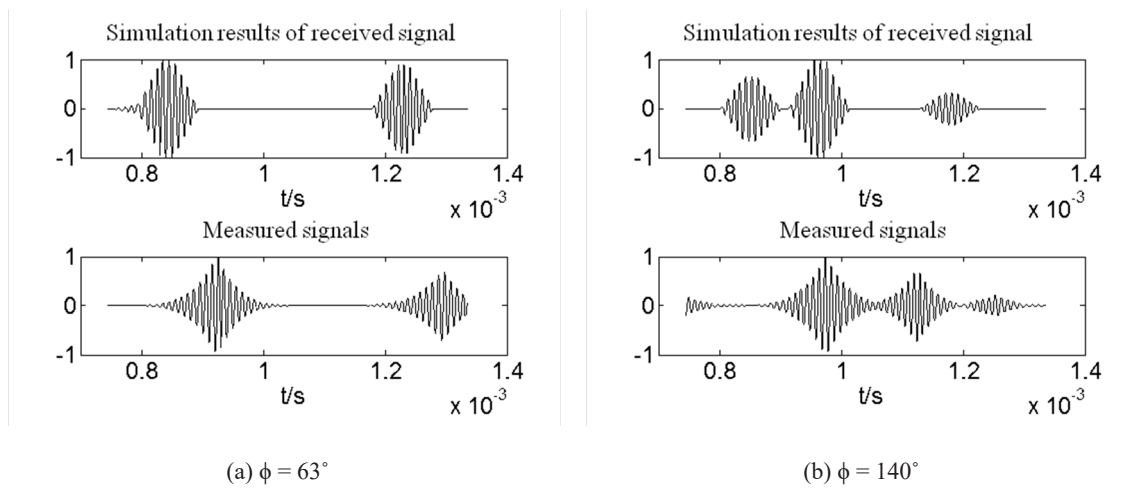
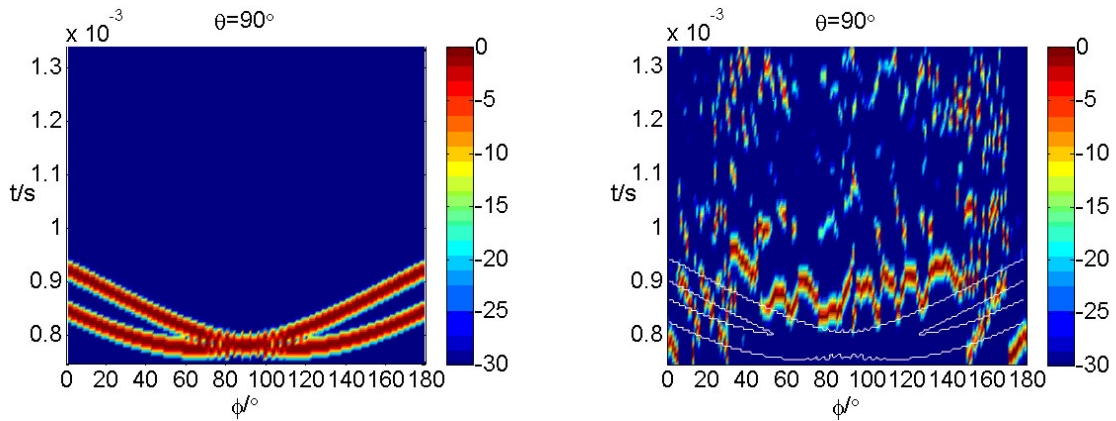


Fig. 14. Received signal of receiver with different angle

3.5 Comparison in Theoretical and Experimental with $\theta = 90^\circ$

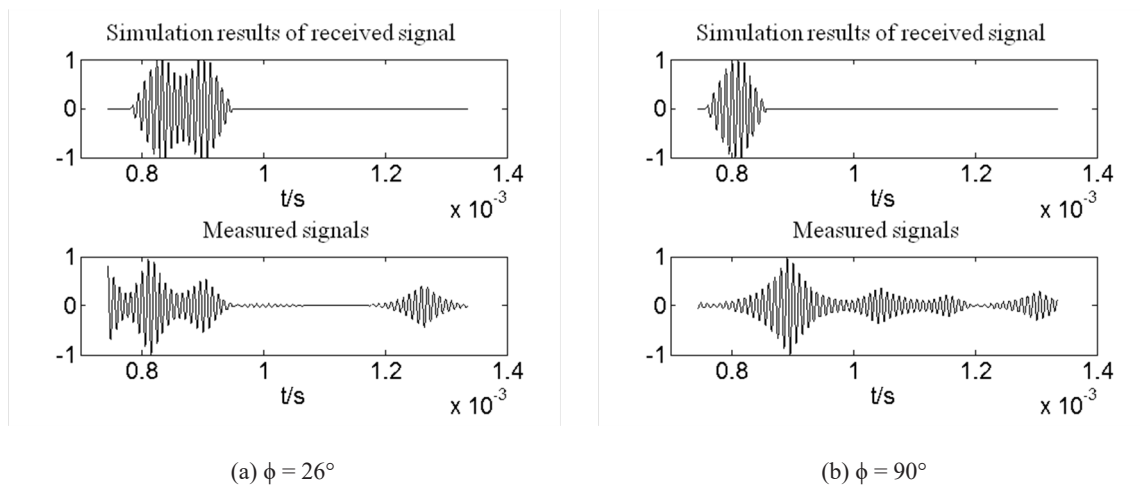
Fig. 15 and Fig. 16 shows the result of only end face scattering. The superposition of signals generated by two highlights in the experiment makes it unstable in time. The calculation results of the simulation are based on a rigid cylinder as the model, while the experiment uses a cylindrical shell, which causes echoes to be generated at both the front and rear ends of the column. This is particularly evident when the target is perpendicular to the reference line, making the actual received signal more complex than the simulation results.

In the experiment, the appearance of elastic highlights can also cause differences between the theoretical model and the measured results. The rotation error caused by manual operation and the system jitter after movement are also important parts that cannot be ignored.



(a) Simulation calculation results of geometric highlights (b) Comparison of experimental and theoretical highlights

Fig. 15. Comparison in theoretical and experimental with $\theta = 90^\circ$



(a) $\phi = 26^\circ$

(b) $\phi = 90^\circ$

Fig. 16. Received signal of receiver with different angle

4 The Second Experiment of Sound Field Measurement in a Bistatic System

Considering the errors caused by manual instability and environmental factors in the previous experiment, the second experiment was conducted in an anechoic water tank with an automatic rotation device. The system layout is shown in Fig. 17, with the transmitter pointing towards the end face of the steel column shell, and the three receivers forming 0-degree, 30-degree, and 60-degree angles with the reference line. The cylindrical target is located under a wheel with an automatic rotation device which is used to slowly rotate the target. The transmitted signal is a 100 kHz CW pulse signal. The receiver always collects the signal until the end of the rotation. In Fig. 18, θ represents the angle between the cylinder busbar and the reference line, and ϕ represents the angle formed by the receiver direction and the reference line. The processing results are shown as follows.

From Fig. 18 to Fig. 23, it can be seen that most of the highlight positions can be well matched in terms of angle and time. It is thus clear that scattering highlight model describes the target scattering field well within a certain range. The second group of experiments showed relatively ideal results due to the use of automatic rotation, which reduced errors caused by manual operations. Therefore, the theory is in good agreement with the experiment.

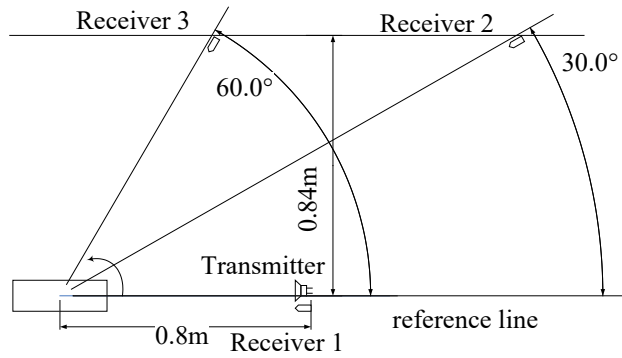
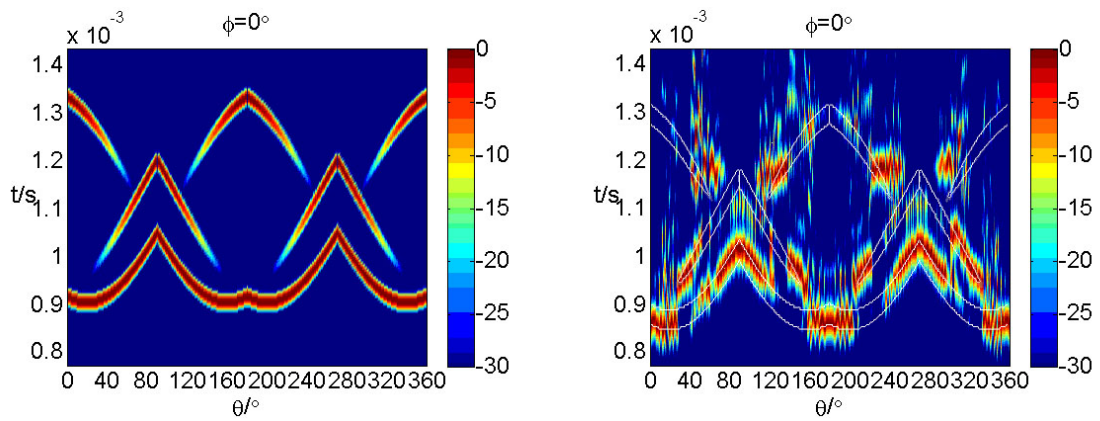
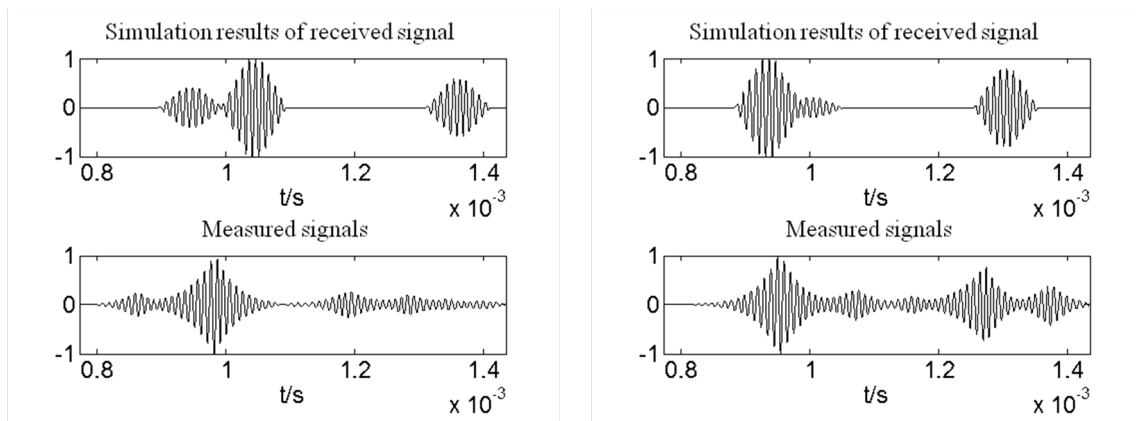


Fig. 17. Deployment of experiment



(a) Simulation calculation results of geometric highlights (b) Comparison of experimental and theoretical highlights

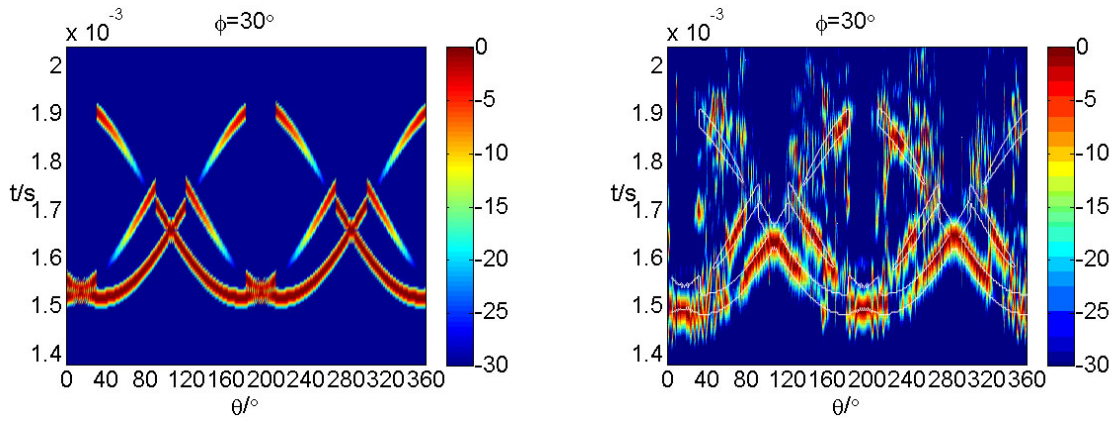
Fig. 18. Comparison in theoretical and experimental with $\phi = 0^\circ$



(a) $\theta = 40^\circ$

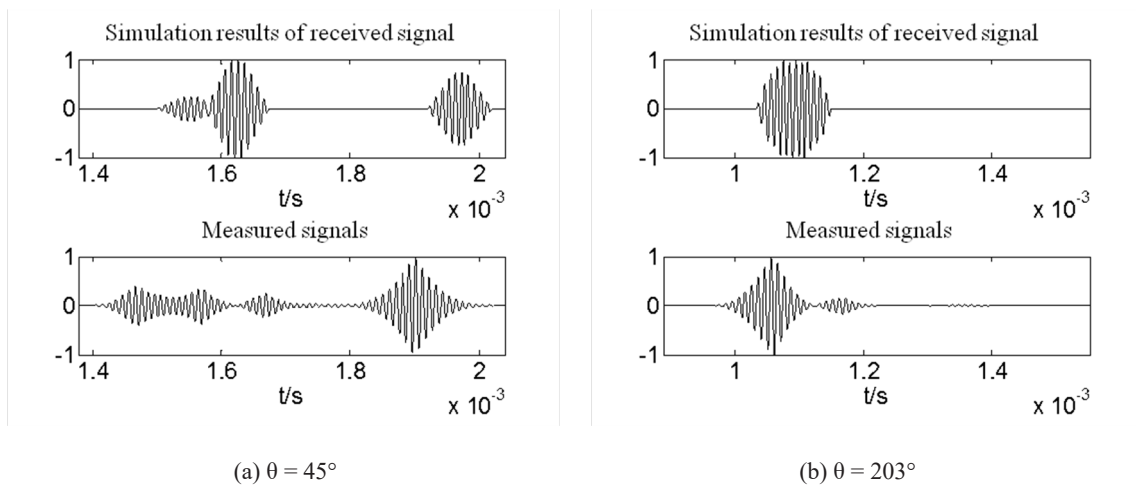
(b) $\theta = 153^\circ$

Fig. 19. Received signal of receiver with different angle



(a) Simulation calculation results of geometric highlights (b) Comparison of experimental and theoretical highlights

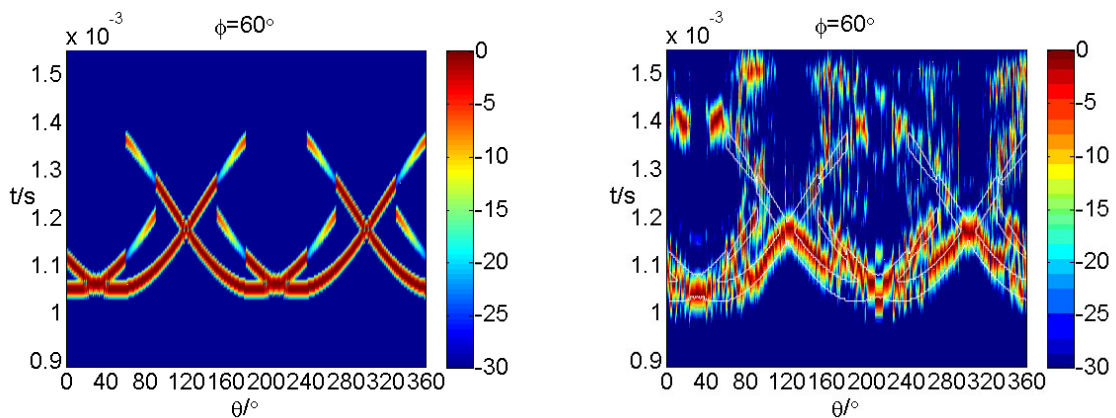
Fig. 20. Comparison in theoretical and experimental with $\phi = 30^\circ$



(a) $\theta = 45^\circ$

(b) $\theta = 203^\circ$

Fig. 21. Received signal of receiver with different angle



(a) Simulation calculation results of geometric highlights (b) Comparison of experimental and theoretical highlights

Fig. 22. Comparison in theoretical and experimental with $\phi = 60^\circ$

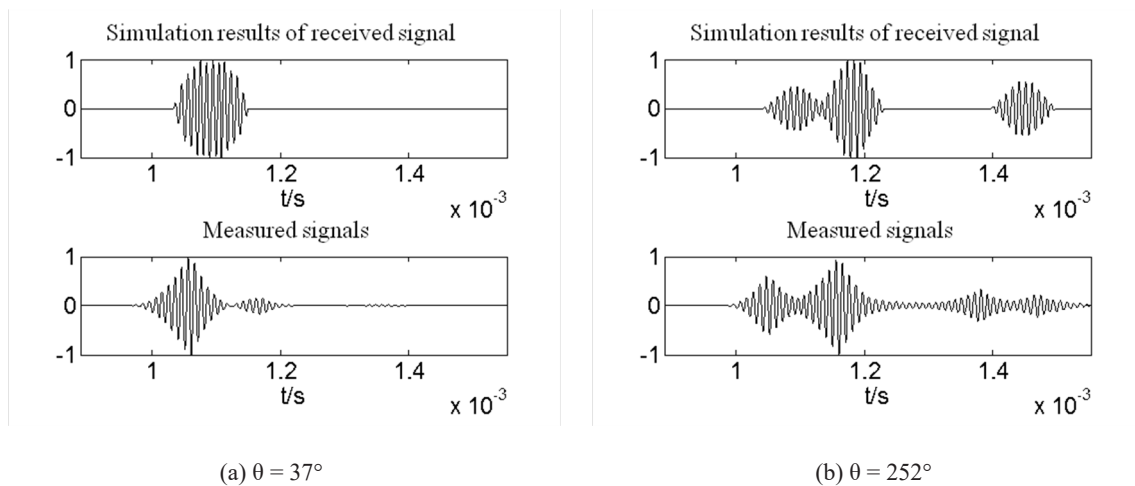


Fig. 23. Received signal of receiver with different angle

5 Analysis of Experimental Results

It should be noted that the Kirchhoff approximation does not have high accuracy in calculating the scattering characteristics of targets in the bistatic system.

Firstly, in the calculation, only the information of the target bright area in the system is considered, while the information of the dark area is ignored, so it is not applicable for conditions with large separation angles. Therefore, in the experiment, the separation angle is less than 90-degree, and within this range, the scattering characteristics of the target in the bistatic system of the highlight model are calculated.

In addition, as a geometric acoustic approximation, the accuracy of the calculation results is directly proportional to the frequency of the sound wave. In practice, the frequency of sound waves is much lower than that of light, which inevitably leads to errors.

Third, a slight deviation between the actual propagation process of sound waves and the theoretical results may result in a time difference between the theoretical and experimental highlights. During simulation, it is approximated as a plane wave, but in reality, both the transmitter and receiver are located at a finite distance, which can cause a deviation in the position of the echo.

Fourth, the theoretical simulation calculation adopts a rigid surface approximation which only considering geometric scattering. The experimental target is elastic materials, which will introduce the influence of elastic scattering. Surrounding waves and shell scattering will cause some scattered waves received at certain positions to deviate from the theoretical simulation results.

Finally, environmental noise and direct sound wave are also important factors affecting the results.

Despite the various adverse factors mentioned above, it can still be seen from the experimental results that the simulation results of the split highlight model are in good agreement with the experimental measurement results, which proves the correctness of the highlight model in bistatic system. The bistatic system highlights model proposed in this article can be used to predict its scattering characteristics of bistatic system in combination with the actual target characteristics.

6 Conclusion and Prospect

6.1 Conclusion

When calculating the high-frequency acoustic scattering field, the applicability of the analytical solution obtained by the wave acoustics method is poor. Therefore, this paper studies the optical approximation for calculating the scattering field, the problem of bistatic acoustic scattering from a finite length rigid cylinder was analyzed based on the Kirchhoff approximation. Based on the calculation results, extend the highlight model to the bistatic

system. When calculating the scattered acoustic field of a target in a bistatic system, the target can be equivalent to several highlights based on certain characteristics of the target, and the received signal consists of these highlights.

Finally, an experiment was conducted to measure the scattered acoustic field of the bistatic system. Under fixed transmitter and target conditions, experiments were conducted to measure the received signal of the receiver rotating around the target, as well as the received signal of the target rotating under multiple split angles. A comparison was made between the experimental results and the theoretical simulation results of the full angle pseudo color image. The comparison between measured signals and simulated signals indicates that the highlight model of bistatic system can describe the scattering characteristics of the target to a certain extent better. In the article, only geometric highlights were simulated, and it can be foreseen that with a full understanding of the target, the highlight model of bistatic system can accurately express the sound field.

6.2 Prospect

In the calculation of scattering systems, most current numerical algorithms are effective at low frequencies, while optical approximations can be used at high frequencies. At present, research on scattering has focused more on theory and less on experimental verification. At the same time, most studies have focused on the monostatic case, with less exploration on the bistatic case. There is great potential for exploring the highlight model under the scattering system conditions proposed in this article, provided that there is sufficient understanding of the target and source. For example, by combining elastic wave scattering theory with highlight model of scattering system, a more comprehensive scattering highlight model can be obtained. On the side, a model library of multiple targets highlight models of scattering system can also be established, which could greatly simplify the calculation of scattering problems.

References

- [1] W.-L. Tang, D.-Zh. Chen, Echo structure of sound scattering by a finite elastic cylinder in water, *Acta Acustica* 13(1) (1988) 29-37.
- [2] W.-L. Tang, Calculation of acoustic scattering of a nonrigid surface using physical acoustic method, *Acta Acustica* 18(1) (1993) 45-53.
- [3] X.-K. Li, Characteristics of underwater object, *Technical Acoustics* 18(A11)(1999) 51-52.
- [4] J. Fan, J.-L. Li, T. Liu, W.-L. Tang, Transition characteristics of echoes from complex shape targets in water, *Journal of Shanghai Jiaotong University* 36(2)(2002) 161-164.
- [5] G.-B. Wang, L.-H. Peng, Studies on Scattering from a Rigid Sphere in a Shallow Water Wave-Guide, *Periodical of Ocean University of China* 35(3)(2005) 515-520.
- [6] G. Wen, M. Shi, X.-B. Zhang, Zh.-L. Xuan, The study of high-frequent echo characteristics from non-rigid targets near an interface, *Journal of Detection & Control* 30 (1)(2008) 66-69.
- [7] W.-J. Chen, H. Sun, A shooting and bouncing beams method for calculating the acoustic scattering field of concave targets, *Acta Acustica* 38(2)(2013) 147-152.
- [8] K.-N. Wei, W. Li, M. Lei, Y.-B. Chai, The low-frequency acoustic scattering characteristics study on underwater targets by the coupled boundary element method, *Ship Science and Technology* 36(10)(2014) 32-36.
- [9] T. Zhu, Research on low-frequency scattering characteristics of underwater targets, [dissertation] Shanghai Jiao Tong University, 2008.
- [10] H.-J. Xiong, B.-Ch. Yuan, H.-K. Zhan, Y.-B. Luo, Simulation of acoustic scattering field targets based on approximate Kirchhoff Formula, *Torpedo Technology* 21(5)(2013) 375-377.
- [11] W.-L. Tang, Highlight model of echoes from sonar target, *Acta Acustica* 19(2)(1994) 92-100.
- [12] J. Fan, T. Liu, W.-L. Tang, The structure of highlight echoes due to specular reflection from shells of immersed target, *Technical Acoustics* 21(4)(2002) 153-157,170.
- [13] Ch.-H. Zhao, T. Hu, Zh.-W. Fu, Simulation on acoustic scattering feature of underwater target, *Applied Science and Technology* 34(6)(2007) 1-4.
- [14] P. Ren, Analysis on back scattering wave structure of elastic cylindrical shell, [dissertation] Harbin Engineering University, 2007.
- [15] Q. Qi, H. Chen, Simulation of the echoes from underwater elastic spherical shells, *Computer Simulation* 25(9)(2008) 16-19,61.
- [16] G.-L. Cheng, M.-M. Zhang, G.-J. Xu, Echo modeling and imaging for underwater typical target in far-field with large rotation angle, *Journal of Wuhan University of Technology (Transportation Science & Engineering)* 32(6)(2008) 1091-

- 1093,1124.
- [17] Y. Xu, B.-CH. Yuan, Q. Li, Modeling and simulation of echoes from mines near an interface based on highlight model, in: Proc. 2011 Asia-Pacific Youth Conference on Communication, 2011.
 - [18] T.-L. Sun, H. Sun, Quasi-Lamb wave for a submerged elastic cylindrical shell, *Journal of Vibration and Shock* 32(19) (2013) 187-191.
 - [19] ZH.-R. Meng, X.-F. Wang, Zh.-W. Lv, The caculation of acoustic field of the cylinder and smooth surface in bistatic, in: Proc. 2020 The 7th International Conference on Computer-Aided Design, Manufacturing, Modeling and Simulation, 2020.